Progress In Electromagnetics Research C, Vol. 85, 51–62, 2018

A Novel Wide-Band Miniaturized Microstrip Patch Antenna by Reactive Loading

Li Wang*, Rui Zhang, Chang Liang Zhao, Xi Chen, Guang Fu, and Xiao-Wei Shi

Abstract—In this paper, a novel miniaturized circularly polarized (CP) antenna is proposed for the use in B3 band of Compass Navigation Satellite System (CNSS). The primary radiator is a hexagon patch with four bending strips. A shorting pin is loaded with each strip to miniaturize the dimension of the proposed antenna, which achieves a small electrical size of $0.11\lambda \times 0.11\lambda \times 0.068\lambda$ (λ being the wave-length in free space at 1.268 GHz). In order to improve the bandwidth, Y-shaped coupled patches and bending-strips, which act as reactive loading, are coupled to an octagon patch. Four coupled bending-stubs with same turning directions of bending-strips are sequentially placed at the edge of the octagon patch to enhance CP performance. Finally, a prototype of the antenna is implemented and measured. The experimental results reveal that the proposed antenna achieves impedance bandwidth (IBW) of 19.6% (1.175–1.430 GHz) for $|S_{11}| \leq -10$ dB and 3-dB axial-ratio bandwidths (ARBW) of 27.5% (1.000–1.320 GHz). The radiation efficiency is more than 75%, and the gain keeps above 1.98 dBic over the B3 band. Thus, the proposed antenna can be a good candidate for the applications of CNSS.

1. INTRODUCTION

Nowadays, GNSS has been used in various fields, such as navigation for vehicles, military applications and scientific surveys about geographical environment. Due to the confined space of application platforms, compact antennas are urgently demanded. A few approaches have been investigated to miniaturize antennas [1]. Firstly, employing high permittivity substrate is a simple way to achieve miniaturization. In [2–4], antennas were etched on a substrate with high permittivity ($\varepsilon_r = 10.2$). Hence, their horizontal sizes were all less than 0.1λ. Unfortunately, this kind of technique brought common drawbacks, like low polarization purity and high-cost. Secondly, loading slots on the radiator is also utilized in [2–5] to reach the tiny size by giving capacitive loading to the patch. The annular ring with rectangular slots and complementary split-ring resonator (CSRR) were utilized to achieve the miniaturization in [2, 3]. Owing to the poor polarization purity resulting from slots, the antenna in [2] showed narrow ARBW of 2.49%. Particularly, as studied in [5], the size ($\Phi = 0.2\lambda$) of a circular patch antenna with ARBW of 2.2%, was reduced through six pairs of symmetric slits embedded along the radiation patch. Thus, slotting on patch suffers from common disadvantage of narrow ARBW. Similarly, slotting on the ground can be another efficient method to reduce the resonant frequency of patch antennas [6–8]. As presented in [6], the application of slotted ground achieved a significant reduction to the size of antenna ($0.21\lambda \times 0.14\lambda$). However, this method requires a relatively large ground, which increases the dimension of the antenna.

Thirdly, folding and shorting techniques are efficient approaches to realize miniaturization [9–12]. Owing to the extended electrical length through folding the patch, this method can obviously reduce the horizontal size of patch. In [9, 10], the employed multilayer configuration realized a significant size

Received 16 May 2018, Accepted 21 June 2018, Scheduled 29 June 2018

* Corresponding author: Li Wang (wangkalina@yeah.net).

The authors are with the Science and Technology on Antenna and Microwave Laboratory, Xidian University, Xi'an, Shaanxi 710071, China.

reduction with a dimension of $0.2\lambda \times 0.2\lambda$. Another case of this method is virtually shorted-patch antenna (VSPA) [13, 14]. This concept was first proposed in [13], with the short-circuited L-shaped strips coupled to the patch instead of connected to the patch directly, and an LC loading effect was provided. Thus, the reduction of resonant frequency could be obtained. As investigated in [13], a VSPA achieved a small size ($0.1\lambda \times 0.1\lambda$) by utilizing the parasitic structures and high permittivity substrate ($\varepsilon_r = 10$), whereas the antenna showed a poor performance at IBW and ARBW, which were 3.25% and 0.682%, respectively. Similarly, Reference [14] discussed a miniaturized antenna with a size of $0.1\lambda \times 0.1\lambda$, while the IBW and ARBW were only 1.1% and 0.3%. Thus, a few approaches have been investigated to reach wideband performance. As shown in [15, 16], stubs were employed to generate dual resonant frequencies to enlarge the bandwidth by employing a stub. Meanwhile, a wideband operation was obtained by adopting a special shape monopole [17]. However, all the antennas introduced above cannot maintain a tiny size and stable impedance bandwidth at the same time.

In this paper, a novel concept to design a miniaturized antenna with band enhancement is presented. By utilizing parasitic bending-shorting-strips referred from [12], the overall antenna volume achieves only $0.11\lambda \times 0.11\lambda \times 0.068\lambda$. Meanwhile, the bandwidth of the antenna decreases as the size decreases. In order to improve the IBW, a few techniques of loading reactance have been utilized in this antenna, such as a Y-shaped coupled patch, coupled strips and stubs. Furthermore, through bending strips and stubs around the radiation patch symmetrically to preserve polarization purity, a better CP performance is achieved. Measurements were carried out to verify the simulations, and the measured results indicate good agreement with the simulated ones.

2. ANTENNA CONFIGURATION

Figure 1 depicts the 3D-view configuration of the proposed antenna. The proposed antenna consists of two portions: upper PCB and lower PCB, connected by feeding pins and shorting pins. For preserving radiation efficiency of the proposed antenna, a low-loss substrate F4B ($\varepsilon_r = 2.65$, $\tan\delta = 0.001$) with thickness of 1 mm is utilized for the upper PCB. To maintain the miniaturization, the feeding network is etched on a 1 mm-thickness FR4 substrate with relatively high permittivity ($\varepsilon_r = 4.4$, $\tan\delta = 0.002$).

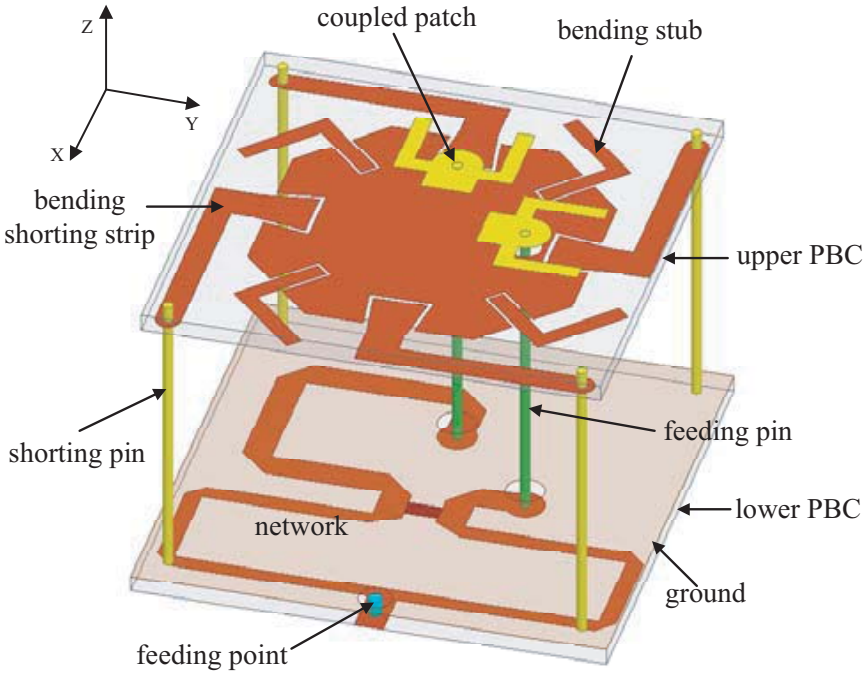

Figure 1. 3D-view configuration of proposed antenna.

The radiator contains an octagonal patch, bending shorting strips and bending stubs, etched on the bottom surface of upper PCB. Four bending shorting strips, coupled to the patch, are symmetrically embedded at the long edge of octagonal patch. Meanwhile, four bending stubs are placed sequentially at the short edge. The widths of gaps between patch and strips, patch and stubs are decided by parameters G_1 and G_2, respectively. The embedded lengths of strips and stubs are labeled as L_{in1} and L_{in2}. On

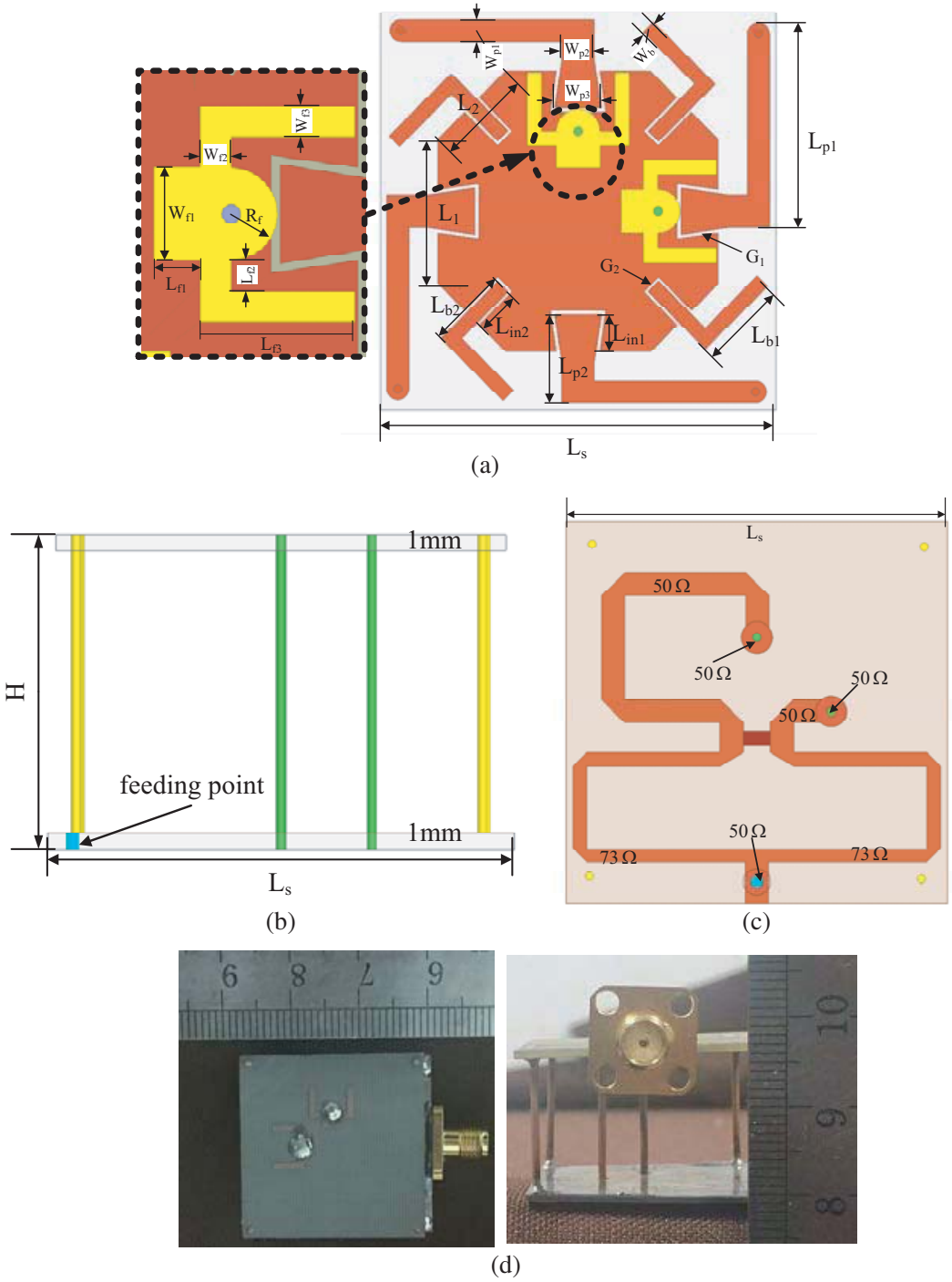

Figure 2. Geometry of the proposed antenna. (a) Top view. (b) Side view. (c) Feeding network. (d) Photograph of the prototype.

the top side of upper PCB, two Y-shape coupled feeding patches are placed orthogonally. The specific parameters about the upper PCB are depicted in Fig. 2(a). As shown in Fig. 1 and Fig. 2(b), one end of the shorting pin is connected to the strip, and the other end is connected to the metal ground on the top side of lower PCB. The coupled-fed patches and the feeding network are connected by feeding pins through apertures between the octagonal patch and ground. The height of antenna is labeled as H. The structure shown in Fig. 2(c) is a Wilkinson feeding network at top side of the lower PCB. To make sure the bandwidth of antenna will be dominated by radiation portion, all the three ports are designed to match with $50\,\Omega$, and the characteristic impedance of each segment is calculated and labeled in Fig. 2(c). The simulated performances of the network are shown in Fig. 3, and the results illustrate that the band of $1.22 \sim 1.32\,\text{GHz}$ for VSWR ≤ 1.10 is obtained. The good transmission coefficients and phases ensure an equal magnitude and 90°-phase difference between ports.

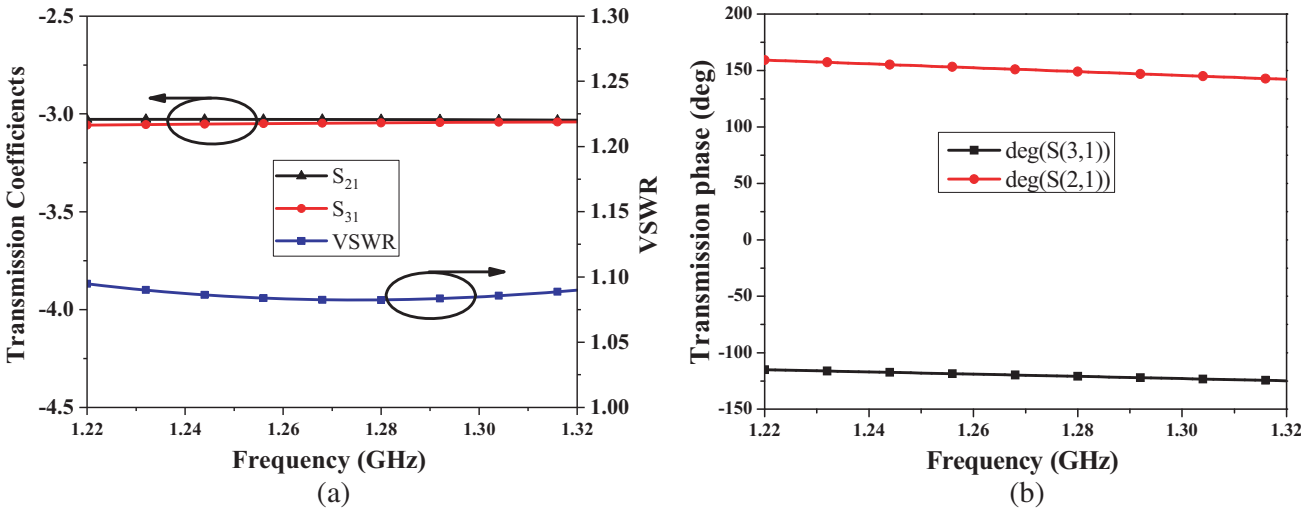

Figure 3. Performance of feeding network. (a) Transmission coefficients and VSWR. (b) Transmission phases.

3. PRINCIPLE AND METHODOLOGY

In this section, the techniques adopted by the proposed antenna are divided into two parts: miniaturization and bandwidth enhancement. Both of them have been studied in detail. According to the order of applied techniques, the processes and comparisons are given as below. Meanwhile, several antenna models are simulated by HFSS 13.0 to help the investigation. Finally, a desired antenna is achieved, and the key parameters have been studied to understand the proposed antenna.

3.1. Miniaturization

In order to achieve a miniaturized size, a few approaches have been utilized to extended the current length in this episode. Three models in Fig. 4 have been built to verify the effect of strips and shorting pins on miniaturization. Initially, a conventional patch antenna with external dimensions of $20 \times 20 \times 16\,(\text{mm})$ is proposed. An octagonal patch is directly connected with feeding pin (Fig. 4, model A), and the longer edge and shorter edge are $L_1 = 9.9\,\text{mm}$ and $L_2 = 6.5\,\text{mm}$, respectively. Owing to the limited dimensions, the resonant frequency of this structure is at 1.97 GHz. To obtain a longer current path, four bending strips are connected to the octagonal patch in the second model (Fig. 4, model B). As indicated in [1], this symmetrical structure can also benefit polarization purity. Through bending strips, the resonant frequency is lowered to 1.76 GHz. Further, because the shorting pin can lower the resonant frequency significantly, four shorting pins are introduced to connect the strips with ground in model C of Fig. 4, which can significantly move resonant frequency to 1.28 GHz. In Fig. 4,

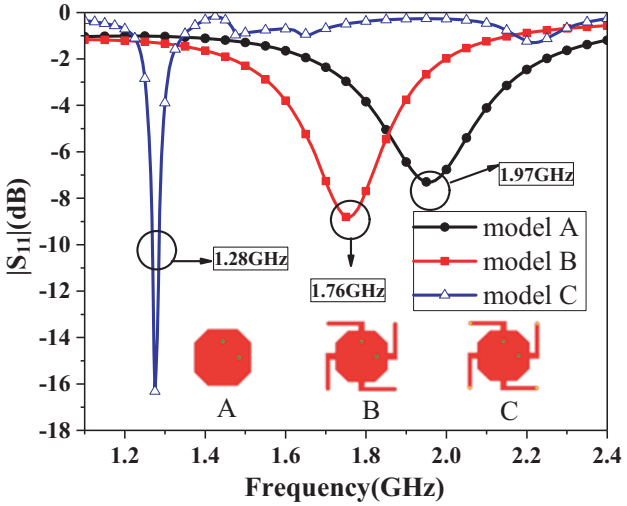

Figure 4. Comparison of $|S_{11}|$s for three type antennas.

the results of comparisons among three models are presented. As shown, resonant frequencies of the models get lower gradually, especially model C. It illustrates that the shorting strips are highly effective to miniaturization of the antenna.

3.2. Bandwidth Enhancement

As discussed in previous part, the shorting pins can reduce the resonant frequency efficiently. Besides, the shorting pins can be regarded as an LC loading. According to circuit theory, the quality factor Q of LC series can be expressed as below:

$$Q = (1/R)\sqrt{L/C} \tag{1}$$

It is known that IBW of the circuit is inversely proportional to the Q-factor. According to the expression, Q-factor will be increased by increasing L, and the shorting pins provide a large L; therefore, the IBW is decreased rapidly in model C. Fig. 5 shows the $|S_{11}|$ of models C–E. The IBW of model C keeps extremely narrow bandwidth. It is well known that IBW enhancement can be achieved through

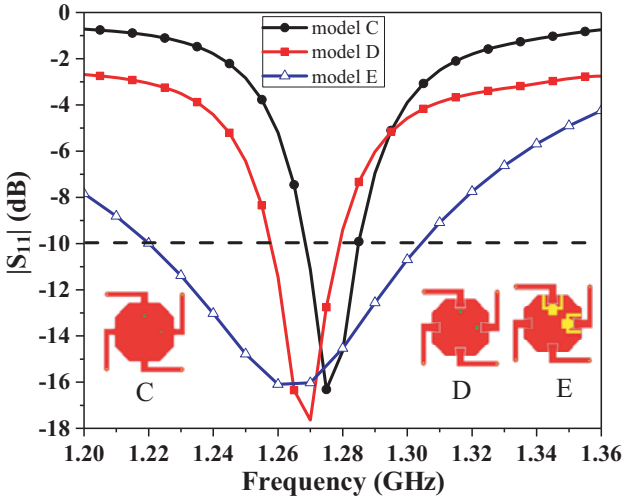

Figure 5. Comparison of $|S_{11}|$s for three type antennas.

introducing slots, which are regarded as capacitive loadings. Firstly, by slotting at the octagonal patch, the bending shorting strips are coupled with the octagon patch instead of connecting directly (model D). The other popular way to enhance impedance matching is by employing the coupled-fed techniques. Secondly, to further enhance IBW, two Y-shape coupled-fed patches are utilized in model E. As shown in function (2), the resonant frequency decreases as L or C increases. Due to the capacitive compensation of slots, the IBW of model D is slightly wider than model C, and the resonant frequency moves to lower band at 1.27 GHz. Obviously, model E achieves the widest IBW of 6%. However, as shown in Fig. 6, the AR of model E shows narrow band and keeps above 1.5 dB. However, a stable and good CP property is also necessary for the GNSS. In order to realize a better CP performance, the models with straight strips and bending strips are investigated. The bending direction is the same as the direction of RHCP (co-polarization), and the total length of the strips is equal to 17.75 mm ($L_{p1} + L_{p2}$). Fig. 6 shows the AR of models E–G. It indicates that the bending strips show better CP performance than straight ones, which means that the same direction between structures and polarization can improve the CP property. So coupled bending stubs are introduced to the antenna, as shown in Fig. 6 (model G). The AR curves indicate that the AR of model G is lower than others, and the ARBW is the widest. Due to the symmetrical structures, bending strips and stubs can enhance the ARBW and maintain the polarization purity, which proves that the proposed antenna can preserve a good CP characteristic.

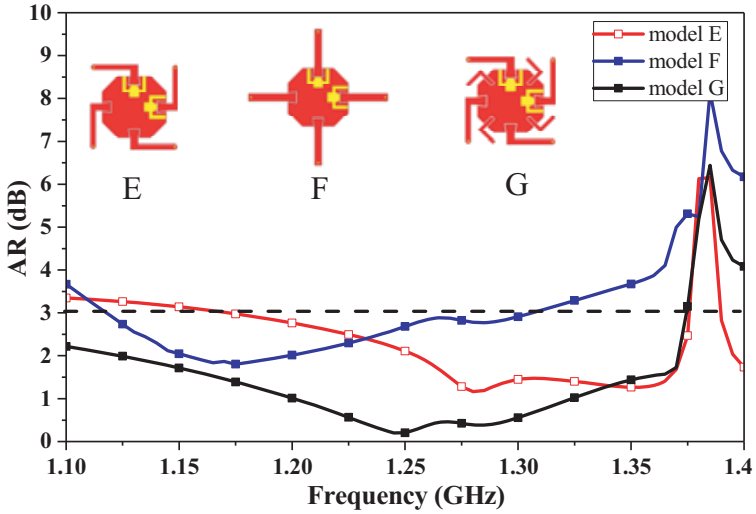

Figure 6. Comparison of ARs for three type antennas.

3.3. Equivalent Circuit and Parametric Study

Semi-analytical techniques [18–21] and equivalent circuit models are efficiency ways to understand microstrip antennas with stubs and slots. Thus, Fig. 8 gives an equivalent circuit model to understand the antenna. The boxes with dotted lines show equivalent circuit components of the bending strips and shorting pins, which can be treated as an LC series circuit. $L1$ is equal to the inductor of the feed pin, and L2 represents the inductor of the Y-shaped patch. The gap between the coupled patch and radiation patch acts as capacitor C3. R1, C1, R2, and C2 are resistors and capacitors of the parallel transmission lines. All the LC resonant circuits, which belong to the proposed structure, enlarge the bandwidth. By tuning the values of the circuit components, the desired operating band can be achieved. Thus, two key factors of the proposed antenna are studied. To study the influence of the Y-shaped patch on the impedance matching, the length of Y-shaped feed patch is investigated and depicted in Fig. 7(b). Fig. 7(b) shows the simulated input impedance versus frequency corresponding to different values of L_{f3}. It is observed that the impedance imaginary part is towards zero, and the real part is stable, when L_{f3} increases, which means that the Y-shaped patch can be a reactive compensation. Here a good impedance match is obtained when $L_{f3} = 5$ mm. The input impedance variation with L_{in1} is shown in

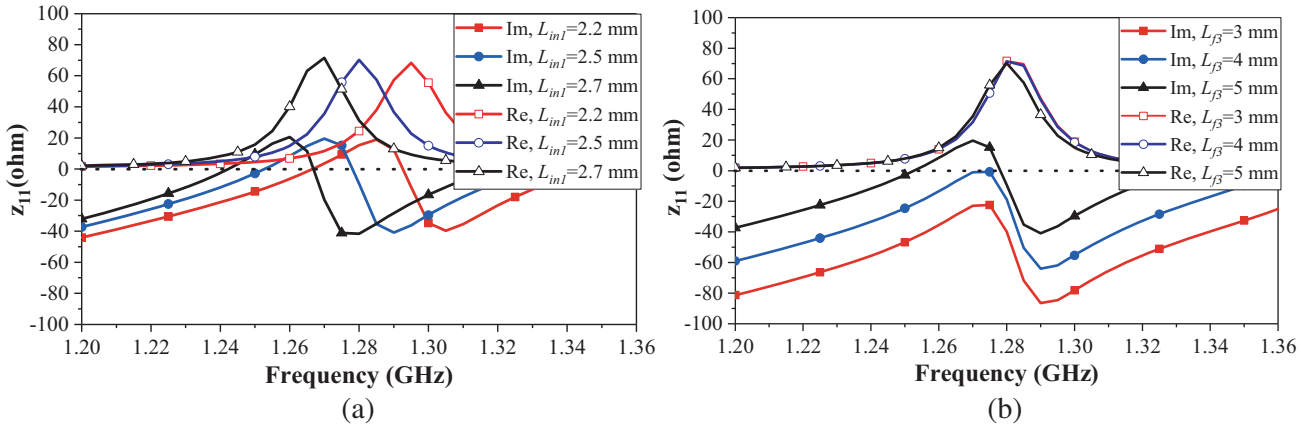

Figure 7. Z_{11}s of proposed antenna. (a) With different L_{in1}. (b) With different L_{f3}.

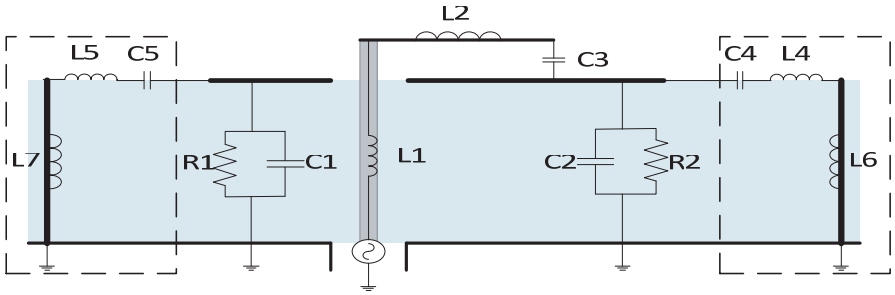

Figure 8. Equivalent circuit model.

Fig. 7(a). Because the coupled bending strips can act as inductors, and the slots are equal to capacitors, the impedance curves show that the resonant frequency moves to lower band, when L_{in1} varies from 2.2 to 2.7 mm. The results show agreement with the function as below. When L and C increase, the resonant frequency f_0 decreases. Finally, with optimum impedance matching, L_{in1} is equal to 2.5 mm.

$$f_0 = 1/\left(2\pi\sqrt{LC}\right) \tag{2}$$

4. RESULT AND DISCUSSION

According to the studied antenna structures and optimized parameters above, a prototype with coupled bending shorting strips and coupled bending stubs is fabricated and measured to validate the simulated results. The final optimized parameters of this prototype are listed in Table 1, and photographs of the fabricated antenna are depicted in Fig. 2(d). The measurements are carried out by using a network analyser AV3672B-S and NSI300V-30X30 far-field measurement system.

Figure 9(a) shows $|S_{11}|$ of the proposed antenna. The measured and simulated IBMs are 19.6% (1.175–1.43 GHz) and 15.9% (1.15–1.37 GHz), respectively. In Fig. 9(a), the radiation efficiencies are depicted. Due to the mismatching with the Wilkinson divider at the side frequency, the proposed antenna shows poor radiation efficiency at high and low bands. However, as depicted in Fig. 10(a), the radiation efficiency more than 75% is obtained during the B3 band. The co-polarization (RHCP) gain and AR versus frequency at broadside are presented in Fig. 10(b) and Fig. 9(b). It is indicated that the gain keeps above 1.98 dBic over B3 band and that 3-dB ARBW of 27.5% (1.000–1.320 GHz) is achieved. As shown in Fig. 11, the major current-density distribution is on the bending-strips, which means that the bending-strips are the main radiators. Two main radiating parts at arbitrary time maintain a stable gain, and symmetrical current ensures a stable radiation pattern. Moreover, the main current-direction

Table 1. Parameters of antenna.

Parameters	L_{p1}	L_{p2}	W_{p1}	W_{p2}	W_{p3}	L_{b1}
Value (mm)	11.75	6	1.5	2.2	3.2	6
Parameters	L_{b2}	L_{in1}	L_{in2}	L_1	L_2	G_1
Value (mm)	4.5	2.5	3	9.9	6.5	0.3
Parameters	G_2	L_{f1}	L_{f2}	L_{f3}	W_{f1}	W_{f2}
Value (mm)	0.2	1.5	1	5	3	1
Parameters	W_{f3}	R_f	L_s	H		
Value (mm)	1	1.5	26.5	16		

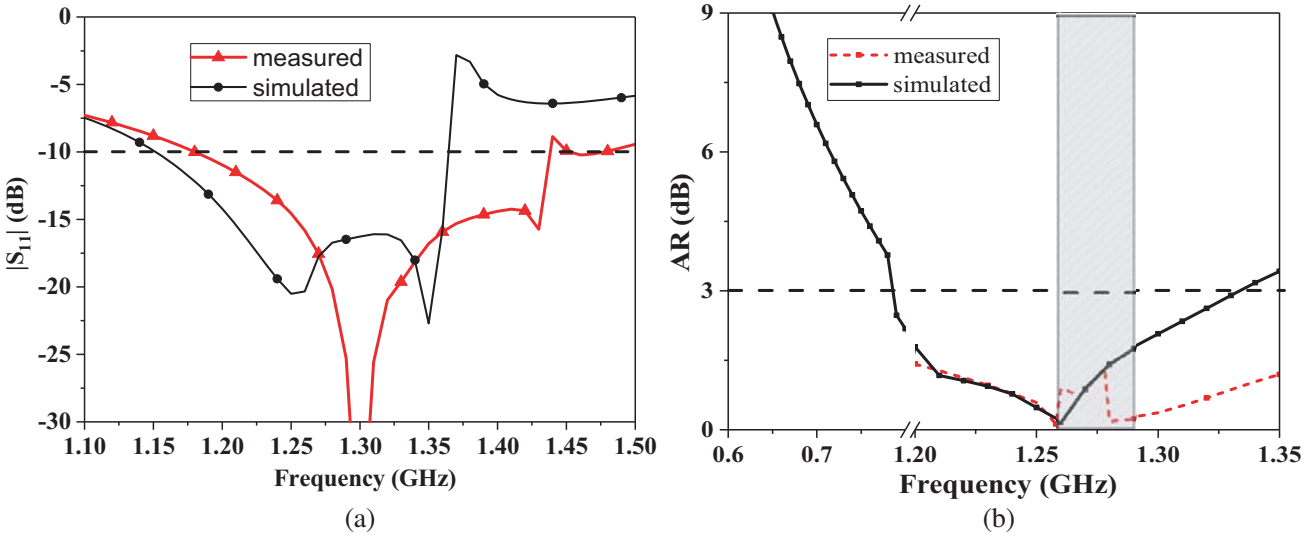

Figure 9. $|S_{11}|$s and ARs at broadside direction. (a) $|S_{11}|$s. (b) ARs.

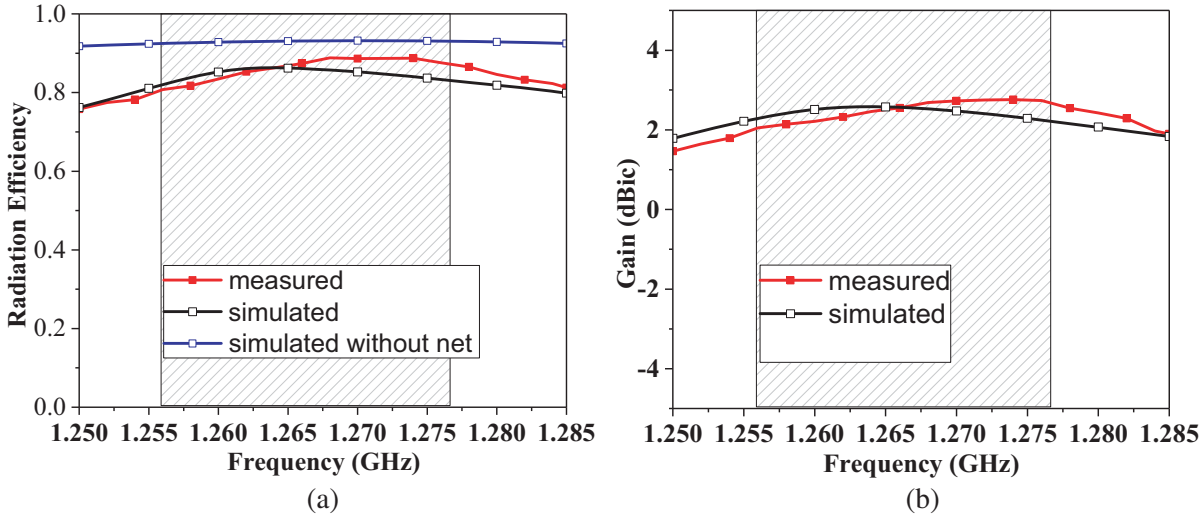

Figure 10. Radiation efficiency and gains at broadside direction of B3 band. (a) Radiation efficiencies. (b) Gains.

of time-dependent rotating is clearly observed, which confirms the RHCP radiation of the proposed antenna.

Figure 12 shows the radiation patterns in two orthogonal elevation planes ($\theta = 0°$ and $\theta = 90°$) at 1.258 GHz, 1.268 GHz and 1.278 GHz. As shown in the pictures, the measured curves agree well with the simulated ones. Because cross polarization is easy to be interfered by the fabricating and testing errors, the measured cross polarization values are slightly different from the simulated ones. To verify the good performance of the proposed antenna, a comparison with other works on impedance bandwidth, ARBW, and dimension is carried out in Table 2. Through the above results, it is indicated that the proposed antenna has an excellent CP performance in the desired band of B3.

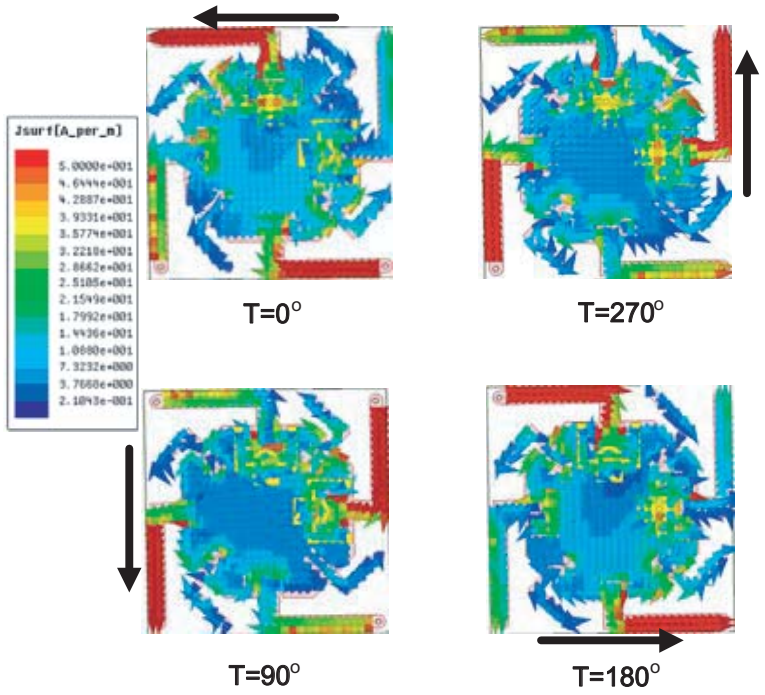

Figure 11. Current distribution at 1.268 GHz with time instant.

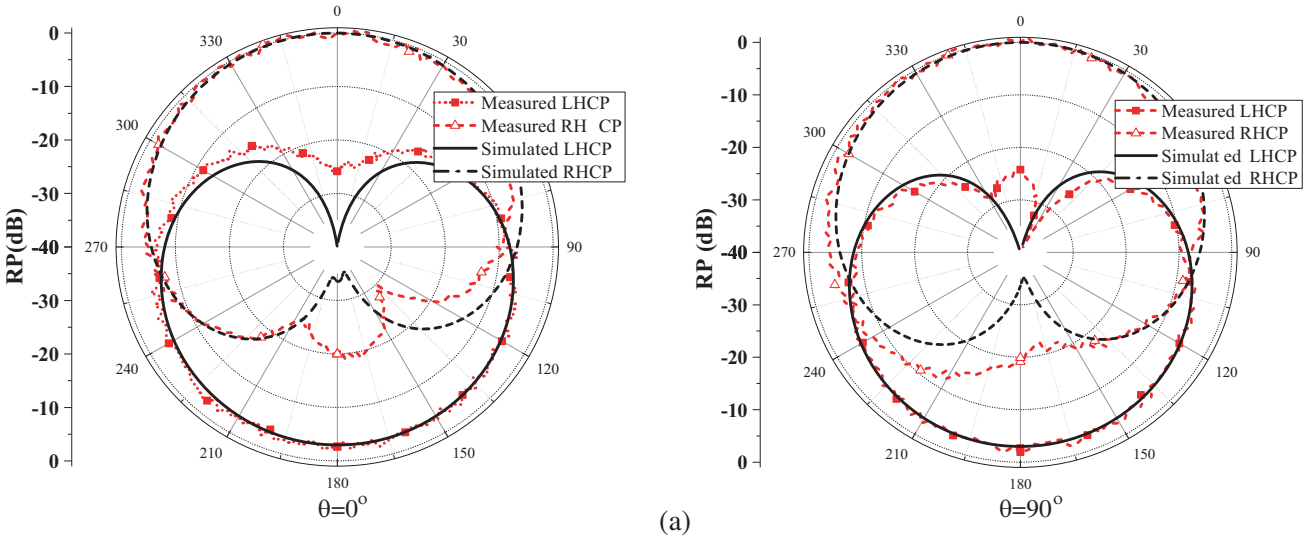

(a)

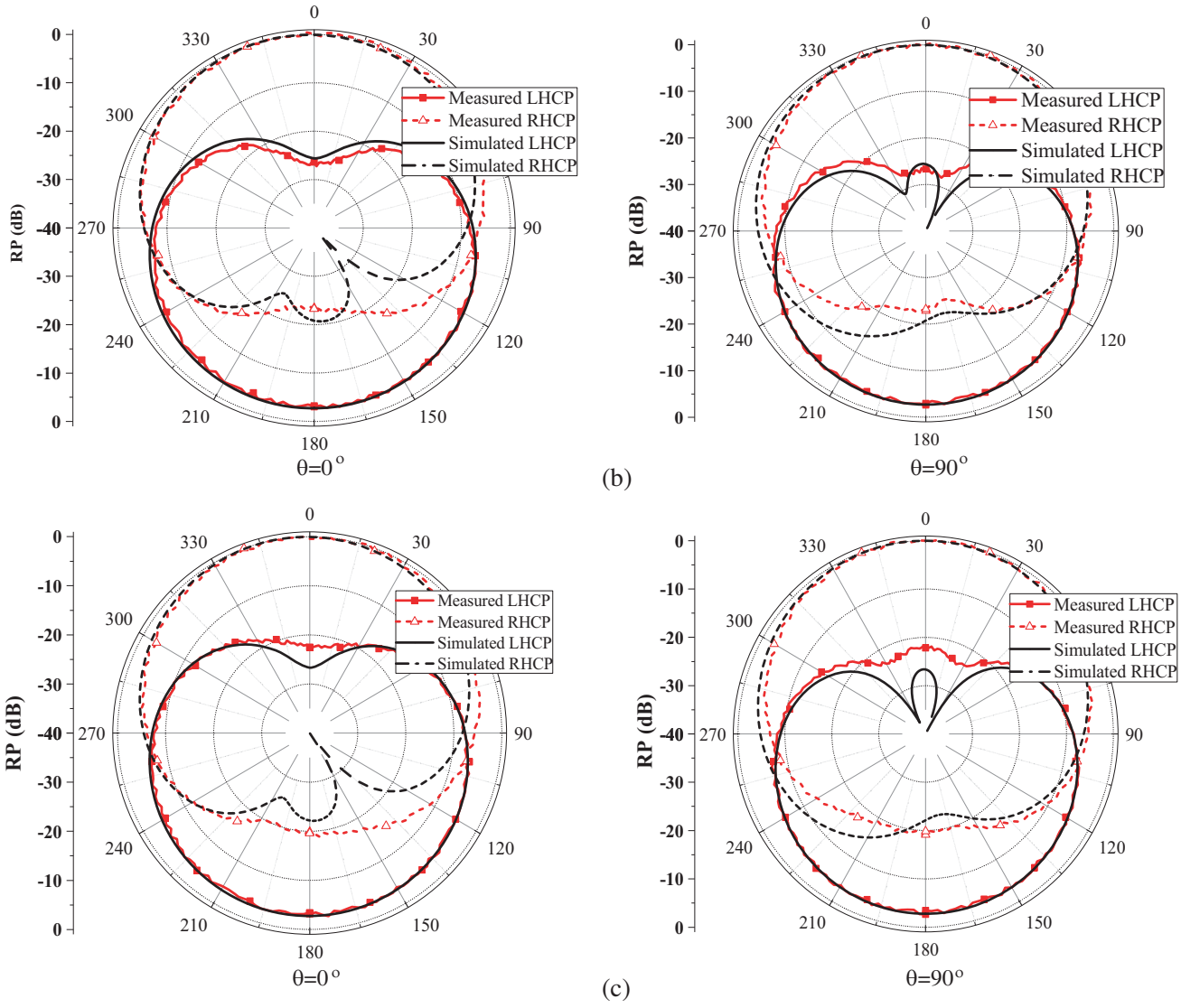

Figure 12. Measured and simulated radiation patterns. (a) 1.258 GHz. (b) 1.268 GHz. (c) 1.278 GHz.

Table 2. Comparison with other works.

Ref.	[12]	[13]	[14]	This work
permittivity	2.2	10	10	2.65
IBW for $\|S_{11}\| \leq -10$ dB	6.4%	3.3%	1.1%	29.6%
ARBW for AR ≤ 3 dB	14.4%	0.7%	0.3%	27.5%
Dimensions	$0.37\lambda \times 0.37\lambda \times 0.15\lambda$	$0.1\lambda \times 0.1\lambda \times 0.026\lambda$	$0.1\lambda \times 0.1\lambda \times 0.016\lambda$	$0.11\lambda \times 0.11\lambda \times 0.068\lambda$

5. CONCLUSION

In this paper, a novel miniaturized circularly polarized (CP) antenna with band enhancement is proposed. Due to the shorting-loading strip, the dimension of antenna is reduced to 0.1λ. However, the bandwidth of the antenna decreases as the dimension decreases. Loading reactance approaches, such as a Y-shaped coupled patch, coupled strips and stub, have been employed in this antenna to achieve a wide band. Furthermore, through the bending strips and stubs around the radiation patch symmetrically to preserve polarization purity, a better CP performance is achieved. Finally, based on the miniaturized size, good CP property and relative wide band, the proposed antenna can be a good candidate for B3 band of GNSS.

ACKNOWLEDGMENT

This work was supported by the National Natural Science Foundation of China (No. 61601351), PRC.

REFERENCES

1. Khan, M. U., M. S. Sharawi, and R. Mittra, "Microstrip patch antenna miniaturisation techniques: A review," *IET Microwaves Antennas & Propagation*, Vol. 9, 913–922, 2015.
2. Li, H., Y. X. Guo, and S. Q. Xiao, "Broadband circularly polarised implantable antenna for biomedical applications," *Electronics Letters*, Vol. 52, No. 7, 504–506, 2016.
3. Ramzan, M. and K. Topalli, "A miniaturized patch antenna by using a CSRR loading plane," *International Journal of Antennas and Propagation*, Article ID 495629, 2015.
4. Liu, C. R., Y. X. Guo, and S. Xiao, "Capacitively loaded circularly polarized implantable patch antenna for ISM band biomedical applications," *IEEE Transactions on Antennas & Propagation*, Vol. 62, No. 8, 2407–2417, May 2014.
5. Zheng, K. K. and Q. X. Chu, "A small symmetric-slit shaped and annular slotted BeiDou antenna with stable phase center," *IEEE Antennas & Wireless Propagation Letters*, Vol. 17, No. 1, 146–149, Jan. 2017.
6. Cho, Y. and H. Yoo, "Miniaturised dual-band implantable antenna for wireless biotelemetry," *Electronics Letters*, Vol. 52, No. 12, 1005–1007, Jun. 2016.
7. Chakraborty, U., S. K. Chowdhury, and A. K. Bhattacharjee, "Frequency tuning and miniaturization of square microstrip antenna embedded with T-shaped defected ground structure," *Microwave & Optical Technology Letters*, Vol. 55, No. 4, 869–872, Apr. 2013.
8. Prabhakar, H. V., et al., "Effect of various meandering slots in rectangular microstrip antenna ground plane for compact broadband operation," *Electronics Letters*, Vol. 43, No. 16, 848–850, Aug. 2007.
9. Podilchak, S. K., et al., "A compact circularly polarized antenna using an array of folded-shorted patches," *IEEE Transactions on Antennas & Propagation*, Vol. 61, No. 9, 4861–4867, Sep. 2013.
10. Podilchak, S. K., A. P. Murdoch, and Y. M. M. Antar, "Compact microstrip-based folded-shorted patches: PCB antennas for use on microsatellites," *IEEE Antennas & Propagation Magazine*, 88–95, Feb. 2017.
11. Kaufmann, T., D. C. Ranasinghe, M. Zhou, and C. Fumeaux, "Wearable quarter-wave folded microstrip antenna for passive UHF RFID applications," *International Journal of Antennas and Propagation*, Article ID 129839, 2013.
12. He, S. and J. Deng, "Compact and single-feed circularly polarized microstrip antenna with wide beamwidth and axial-ratio beamwidth," *Electronics Letters*, Vol. 53, No. 15, 1013–1015, 2017.
13. Hang, W., et al., "Virtually shorted patch antenna for circular polarization," *IEEE Antennas & Wireless Propagation Letters*, Vol. 9, 1213–1216, 2010.
14. So, K. K., et al., "Miniaturized circularly polarized patch antenna with low back radiation for GPS satellite communications," *IEEE Transactions on Antennas & Propagation*, Vol. 63, No. 12, 5934–5938, Dec. 2015.

15. Liu, X. L., Y.-Z. Yin, P. A. Liu, J. H. Wang, and B. Xu, "A CPW-fed dual band-notched UWB antenna with a pair of bended dual-L-shape parasitic branches," *Progress In Electromagnetics Research*, Vol. 136, 623–634, 2013.
16. Liu, W.-C., "Optimal design of dualband CPW-fed G-shaped monopole antenna for WLAN application," *Progress In Electromagnetics Research*, Vol. 74, 21–38, 2007.
17. Wei, Y. Q., Y. Z. Yin, L. Xie, K. Song, and X. S. Ren, "A novel band-notched antenna with self-similar flame slot used for 2.4 GHz WLAN and UWB application," *Journal of Electromagnetic Waves and Applications*, Vol. 25, Nos. 5–6, 693–701, 2011.
18. Valagiannopoulos, C. A., "High selectivity and controllability of a parallel-plate component with a filled rectangular ridge," *Progress In Electromagnetics Research*, Vol. 119, 497–511, 2011.
19. Valagiannopoulos, C. A., "On examining the influence of a thin dielectric strip posed across the diameter of a penetrable radiating cylinder," *Progress In Electromagnetics Research*, Vol. 3, 203–214, 2008.
20. Valagiannopoulos, C. A., "Single-series solution to the radiation of loop antenna in the presence of a conducting sphere," *Progress In Electromagnetics Research*, Vol. 71, 277–294, 2007.
21. Valagiannopoulos, C. A., "Electromagnetic propagation into parallel-plate waveguide in the presence of a skew metallic surface," *Electromagnetics*, Vol. 31, No. 8, 593–605, 2011.